Extremophiles (2006) 10:427–440
DOI 10.1007/s00792-006-0518-z

ORIGINAL PAPER

Marit Sjo Lorentzen · Elin Moe · Hélène Marie Jouve
Nils Peder Willassen

Cold adapted features of *Vibrio salmonicida* catalase: characterisation and comparison to the mesophilic counterpart from *Proteus mirabilis*

Received: 2 December 2005 / Accepted: 31 January 2006 / Published online: 12 April 2006

Abstract The gene encoding catalase from the psychrophilic marine bacterium *Vibrio salmonicida* LFI1238 was identified, cloned and expressed in the catalase-deficient *Escherichia coli* UM2. Recombinant catalase from *V. salmonicida* (VSC) was purified to apparent homogeneity as a tetramer with a molecular mass of 235 kDa. VSC contained 67% heme *b* and 25% protoporphyrin IX. VSC was able to bind NADPH, react with cyanide and form compounds I and II as other monofunctional small subunit heme catalases. Amino acid sequence alignment of VSC and catalase from the mesophilic *Proteus mirabilis* (PMC) revealed 71% identity. As for cold adapted enzymes in general, VSC possessed a lower temperature optimum and higher catalytic efficiency (k_{cat}/K_m) compared to PMC. VSC have higher affinity for hydrogen peroxide (apparent K_m) at all temperatures. For VSC the turnover rate (k_{cat}) is slightly lower while the catalytic efficiency is slightly higher compared to PMC over the temperature range measured, except at 4°C. Moreover, the catalytic efficiency of VSC and PMC is almost temperature independent, except at 4°C where PMC has a twofold lower efficiency compared to VSC. This may indicate that VSC has evolved to maintain a high efficiency at low temperatures.

Communicated by K. Horikoshi

M. S. Lorentzen · N. P. Willassen (✉)
Department of Molecular Biotechnology, Faculty of Medicine, Institute of Medical Biology, University of Tromsø, 9037 Tromsø, Norway
e-mail: nilspw@fagmed.uit.no
Tel.: +47-77-644651
Fax: +47-77-645350

E. Moe · N. P. Willassen
The Norwegian Structural Biology Centre (NorStruct), University of Tromsø, 9037 Tromsø, Norway

H. M. Jouve
Institut de Biologie Structurale, 41 rue Jules Horowitz, 38027 Grenoble Cedex 1, France

Keywords *Vibrio salmonicida* · *Proteus mirabilis* · Catalase · Characterisation · Cold adaptation

Abbreviations VSC: *Vibrio salmonicida* catalase · PMC: *Proteus mirabilis* catalase · Rz: $A_{405\ nm}/A_{280\ nm}$, Reinheitszahl index

Introduction

Bacteria encounter reactive oxygen species (ROS) that are generated as by-products of oxygen-dependent metabolism, such as the superoxide ($O_2^-\cdot$), the hydroxyl radical ($OH\cdot$), and hydrogen peroxide (H_2O_2), or by the first line of defence during host invasion by the attack of granulocytes and macrophages. Stimulated phagocytic cells migrate to areas of infection and release toxic oxygen radicals as antimicrobial agents (Hassett and Cohen 1989). ROS can damage many important components in the cell including DNA, RNA, proteins, and lipids (Cabiscol et al. 2000). Superoxide dismutases (SODs) are able to disproportionate $O_2^-\cdot$, the first ROS generated in the metabolic reduction of oxygen, to O_2 and H_2O_2 (Fridovich 1978). Catalase is important in the last step in this defence mechanism, catalysing the degradation of H_2O_2 into water and molecular oxygen (Nicholls et al. 2001).

Catalases are divided into three main classes of proteins exhibiting significant catalase activity: (1) the monofunctional heme-containing catalases, (2) the bifunctional heme-containing catalase-peroxidases, and (3) the non-heme or manganese (Mn)-containing catalases (Zamocky and Koller 1999). The monofunctional heme-containing or true catalases are further subdivided into three distinct clades based on phylogenetic analysis performed by Klotz et al. (1997). Clade I contains the plant enzymes, one algal representative and one branch of bacterial catalases. Clade II consists only of large subunit catalases of bacterial and fungal origin, while clade III enzymes are all small subunit

catalases from bacteria, archaea, fungi and other eukaryotes.

Due to their high efficiency in hydrogen peroxide detoxification, catalases have been subject of long-term biochemical study. The enzyme is ubiquitous and has been isolated and characterised from many different prokaryotic and eukaryotic organisms, e.g. *Escherichia coli* (HPII) (Loewen and Switala 1986), *Vibrio fischeri* (Visick and Ruby 1998), *Comamonas terrigena* N3H (Zamocky et al. 2004), and *Sinorhizobium meliloti* (Ardissone et al. 2004). Based on these prolonged studies, the catalytic reaction mechanism is well documented.

The overall main reaction catalysed by catalases, $2H_2O_2 \rightarrow 2H_2O + O_2$, is divided into two distinct stages in the reaction pathway of monofunctional heme-containing catalases. The first stage involves oxidation of the heme iron (in heme-containing catalases) using hydrogen peroxide as substrate to form compound I, an oxyferryl species in which one oxidation equivalent is removed from the iron and a second oxidation equivalent from the porphyrin ring to generate a porphyrin cation radical (Nicholls et al. 2001) [reaction (1)].

$$\mathrm{Enz}\left(\mathrm{Por}-\mathrm{Fe}^{\mathrm{III}}\right)+\mathrm{H_2O_2}\rightarrow \mathrm{Cpd\ I}\left(\mathrm{Por}^{+\bullet}-\mathrm{Fe}^{\mathrm{IV}}=\mathrm{O}\right)+\mathrm{H_2O}. \quad (1)$$

The second stage, or reduction of compound I, employs a second molecule of peroxide to regenerate the resting-state enzyme, water, and oxygen [reaction (2)].

$$\mathrm{Cpd\ I}\left(\mathrm{Por}^{+\bullet}-\mathrm{Fe}^{\mathrm{IV}}=\mathrm{O}\right)+\mathrm{H_2O_2}\rightarrow \mathrm{Enz}\left(\mathrm{Por}-\mathrm{Fe}^{\mathrm{III}}\right)+\mathrm{H_2O}+\mathrm{O_2}. \quad (2)$$

Alternatively, compound I can be reduced by one-electron donors (AH) to give rise to compound II with saturated π orbitals, which comes back to the resting state by another one-electron reduction step, as in typical peroxidases [reactions (3 and 4)].

$$\mathrm{Cpd\ I}\left(\mathrm{Por}^{+\bullet}-\mathrm{Fe}^{\mathrm{IV}}=\mathrm{O}\right)+\mathrm{AH}\rightarrow \mathrm{Cpd\ II}\left(\mathrm{Por}-\mathrm{Fe}^{\mathrm{IV}}=\mathrm{O}\right)+\mathrm{A}^{\bullet+}\mathrm{H}^{+}, \quad (3)$$

$$\mathrm{Cpd\ II}\left(\mathrm{Por}-\mathrm{Fe}^{\mathrm{IV}}=\mathrm{O}\right)+\mathrm{AH}+\mathrm{H}^{+}\rightarrow \mathrm{Enz}\left(\mathrm{Por}-\mathrm{Fe}^{\mathrm{III}}\right)+\mathrm{A}^{\bullet+}\mathrm{H_2O}. \quad (4)$$

Catalase compound II is considered to be an inactive species in the H_2O_2 disproportion reaction. Certain small subunit catalases, such as the mammalian and yeast catalases (Nicholls et al. 2001), and the bacterial catalases from *Micrococcus lysodeikticus* (Murshudov et al. 2002) and *Proteus mirabilis* (Gouet et al. 1995) can avoid inactivation to compound II by using NADPH to reduce compound I (Andreoletti et al. 2001) or, according to certain authors, a hypothetical compound II', i.e. compound II with a tyrosyl radical, produced by the spontaneous decay of compound I (Nicholls et al. 2001).

So far, the 3D structures of eleven monofunctional heme-containing catalases have been determined, where six are of bacterial origin: *E. coli* HPII (Bravo et al. 1995), *M. lysodeikticus* (Murshudov et al. 1992), *P. mirabilis* (Gouet et al. 1995), *P. syringae* (Carpena et al. 2003), *H. pylori* (Loewen et al. 2004), and *E. faecalis* (Hakansson et al. 2004). They share a rather high degree of overall structure similarity and are homo-tetrameric enzymes with a relative molecular mass in the range of 200–340 kDa, and each monomer contains a heme prosthetic group (ferric protoporphyrin IX). The three dimensional structures of the true catalases seem to be highly conserved with each subunit forming a characteristic globule with an extended N-terminal arm (Nicholls et al. 2001). Four distinct structural regions can be identified in each subunit: the N-terminal arm, the β-barrel domain, the wrapping domain and the α-helical domain. The quaternary structure is a compact arrangement with the heme-active site deeply buried in the β-barrel domain and with two or three channels providing access of the substrate to each heme group. Each heme pocket is defined by residues from the β-barrel domain, from the wrapping domain and from the N-terminal arm. Heme *b* or protoheme IX is found in all small subunit catalases characterised so far. The large subunit enzymes contain heme *d* as prosthetic groups and the heme is flipped 180° relative to the heme *b* moiety of the small subunit enzymes.

Organisms living at low temperatures have developed different adaptive strategies to cope with this condition. Cold adaptation includes regulation of membrane fluidity, synthesis of specialised molecules such as cold-shock proteins, cryoprotectors and antifreeze molecules, regulation of ion channels permeability, microtubules polymerisation, seasonal dormancy, and maybe most important, modification of enzyme kinetics (Smalas et al. 2000). Cold adapted enzymes are generally characterised by high catalytic activity associated with reduced thermal stability at lower temperatures than their mesophilic counterparts. In addition, there is a shift in the temperature optimum towards lower temperature.

In this work, we describe the identification of the gene encoding catalase from the psychrophilic *Vibrio salmonicida* LFI1238. The recombinant protein *V. salmonicida* catalase (VSC) was expressed and purified in order to perform biochemical analysis. The biochemical characteristics were compared to a mesophilic counterpart, *P. mirabilis* catalase (PMC), to reveal possible cold adapted features of VSC.

Materials and methods

Bacterial strains, plasmids and *Proteus mirabilis* catalase

The strains and plasmids used in this work are listed in Table 1. *V. salmonicida* LFI1238 isolated from cod (*Gadus morhua*) was kindly provided by Elin Sandaker (Norwegian Institute of Fisheries and Aquaculture

Table 1 Strains and plasmids used in this study

Strain	Genotype and source
E. coli UM2	*araC24 leuB6*(Am) *secA206*(aziR) *fhuA23 lacY1 proC83 tsx-67 purE42 glnV44*(AS) *galK2*(Oc) λ^- *trpE38 katE2 xthA15 his-208 rfbD1 mgl-51 argG77 rpsL109*(strR) *glpR201 xylA5 mtl-1 ilvA681 katG15 thi-1 metA160. E. coli* Genetic Stock Centre
E. coli DH5α	F^- ϕ80d*lacZ*ΔM15 Δ(*lac*ZYA-*arg*F) U169 *rec*A1 *end*A1 *hsd*R17(r_k^-, m_k^+) *pho* A *sup*E44 λ^- *thi*-1 *gyr*A96 *rel*A1. Invitrogen
E. coli DH10B	F^- *mcr*A Δ(*mrr-hsd*RMS-*mcr*BC) ϕ80d*lacZ*ΔM15 Δ*lac*X74 *rec*A1 *end* A1 *ara*Δ139 Δ(*ara, leu*)7697 *gal*U *gal*K λ^- *rps*L (Str^R) *nup*G (Grant et al. 1990)
E. coli cc118λpir	Δ(*ara, leu*) *ara*D Δ*lac*X74 *gal*E *pho*A20 *thi*-1 *rps*E *rpo*B *arg*E(*Am*) *rec* A1 λpir phage lysogen (Herrero et al. 1990)
E. coli HB101	*supE*44, Δ(*mcrC-mrr*), *recA*13, *ara*-14, *proA2*, *lacY*1, *galK*2, *rpsL*20, *xyl*-5, *mtl*-1, *leuB*6, *thi*-1. Takara Bio Inc., Japan
Plasmid	Coding gene and source
pVLT49	T7-*polymerase* (Herrero et al. 1993)
pRK2013	RK2 *tra* (Figurski et al. 1979)

Research, Tromsø, Norway). PMC, without bound NADPH, was purified to homogeneity from *P. mirabilis* PR bacteria, as described previously (Jouve et al. 1989), with the improvements proposed by Andreoletti et al. (2003). Purified PMC had a Rz index of 1, a protoporphyrin IX and heme content of 5 and 75%, respectively, as reported by Andreoletti et al. (2003).

Generation of a 500 bp fragment of the *catA* gene

Degenerated oligonucleotide primers (purchased from Invitrogen Life Technologies, Great Britain) were designed from two conserved regions of amino acid sequences in *V. fischeri* and *H. influenzae* catalases. The catalase fragment was generated by PCR using 125 ng genomic *V. salmonicida* DNA as template, and PCR was carried out in a final volume of 50 µl containing 10 mM Tris–HCl, pH 9.0 (25°C), 50 mM KCl, 0.1% Triton X-100, 1.5 mM $MgCl_2$, 0.2 mM dATP, dCTP, dGTP and dTTP, 0.2 µM upstream primer (5′-GCT GAG CGT GAT RTK CGT GGT TT-3′) and downstream primer (5′-GCA TCY GCT TCY GGC ATR ATY TG-3′), and 1.5 U Taq-polymerase (Promega, Madison, WI, USA). PCR-amplification was performed at 94°C for 5 min, 30 cycles of 94°C for 30 s, 60°C for 1 min, and 72°C for 2 min, a final extension step of 72°C for 7 min, and then the reaction mixture was kept at 4°C. The PCR-product was purified using QIAquick PCR Purification Kit (Qiagen, Germany), following the protocol supplied by the manufacturer.

DNA sequencing

DNA sequencing was performed using the PE Biosystems BigDye Terminator Cycle Sequencing Kit Version 3.0/3.1, ABI 377 Genetic Analyser, and ABI Sequence Analysis software Version 3.0, according to the protocol supplied by Applied Biosystems (Foster City, CA, USA).

Southern hybridisation to BAC-library of *Vibrio salmonicida*

Southern hybridisation of a *V. salmonicida* BAC-library (Molecular Engines Laboratories, France) was performed using DIG High Prime DNA Labelling and Detection Starter Kit II (Roche, Penzberg, Germany), and Lumi-Imager F1 with LumiAnalyst 3.0 software (Boehringer Mannheim, Germany), according to the manufacturer's manual. A 500 bp catalase PCR-product was used as probe. The hybridisation temperature was set to 42°C.

Isolation of BAC-clone, amplification of 500 bp fragment and sequencing of the complete *catA* gene

The BAC clones identified by Southern hybridisation were grown overnight in Luria–Bertani (LB) liquid medium containing chloramphenicol (12.5 µg ml^{-1}). The BAC DNA containing the *catA* gene was purified using NucleoBond BAC 100 (Macherey-Nagel, Duren, Germany), following the protocol from the supplier. The 500 bp catalase fragment was generated by PCR using 600 ng BAC DNA as template, and sequencing was carried out as described above. Primer walking was performed on the BAC-clone to obtain the complete sequence of the *catA* gene. Forwards primer sequences were: 5′-GAC AGT ATT GAT AAC CAA GAC TTC C-3′, 5′-CAC GTA ACC TAA ATG GTG TGC C-3′, 5′-CTC AAC AAG GCA TTA AAA ACC T-3′, 5′-GAC CAA GGT CAA TGG GCA GAA-3′ and 5′-GAA GAT TAC TTC TCA CAA CCG G-3′. Reverse primer sequences were: 5′-GGT ATT GTT ACC CGC TAA ATC CCA G-3′, 5′-TTT CTA AAA ACC AAA CAT CTT GC-3′, 5′-GTG CGA GGA TCA CGT TTT ACT G-3′and 5′-TAC CCT GCA ACC AGT GTA GGA T-3′. The primers were purchased from Invitrogen Life Technolgies and Sigma-Genosys (Great Britain).

Sequence analysis

Blast searches were performed using the NCBI server (http://www4.ncbi.nlm.nih.gov/entrez/query.fcgi). Alignments were produced by ClustalW (Thompson et al. 2000) and visualised by using BioEdit (Hall 1999).

Construction of expression vectors

Cloning of the *catA* gene containing nucleotides encoding a C-terminal His-tag into the expression vector pET-DEST42 (Gateway Technology, Invitrogen, Carlsbad, CA, USA) was performed following the protocol supplied by the manufacturer. *attB*-PCR forwards and reverse primer sequences used were 5′-GGG GAC AAG TTT GTA AAA AAA GCA GGC TTC GAA GGA GAT AGA ACC ATG AGT AAG AAA TTA ACG ACA GCA GCA-3′ and 5′-GGG GAC CAC TTT GTA CAA GAA AGC TGG GTC CGA ATT ATA TTC ACT GAT ATC GAA-3′, respectively. Both primers were obtained from Sigma-Genosys. The *katE, katG* negative *E. coli* UM2 (*E. coli* Genetic Stock Centre, New Haven, CT, USA) was transformed with the expression vector. *E. coli* strain UM2 was grown on LB agar plates or in LB liquid medium supplemented with streptomycin (25 μg ml^{-1}). *E. coli* UM2 does not contain T7-polymerase which is required for expression from pET-DEST42. Mobilisation of pVLT49 containing T7-polymerase by pRK2013 and conjugation into *E. coli* UM2 pET-DEST42*catA* was performed as follows: 1.5 ml overnight culture of *E. coli* UM2 pET-DEST42 *catA* grown in LB liquid medium containing ampicillin (100 μg ml^{-1}), 1 ml *E. coli* cc118 pVLT49 grown in LB liquid medium containing chloramphenicol (20 μg ml^{-1}), and 1 ml *E. coli* HB101 pRK2013 grown in LB liquid medium containing kanamycin (50 μg ml^{-1}) were pelleted for 2 min at 13,000*g* in eppendorf tubes and serially resuspended in a total of 150 μl LB+ medium. The mixture was plated on a 0.45 μm filter on a LB agar plate and incubated at 37°C for about 4 h. The filter was transferred to an eppendorf tube, the culture washed off with 2 ml LB containing ampicillin and chloramphenicol (100 and 12.5 μg ml^{-1}, respectively), and then incubated with shaking at 37°C for 1 h. Dilutions (10^{-1}, 10^{-2} and 10^{-3}) of the conjugation mixture were plated on LB agar plates containing ampicillin and chloramphenicol (100 and 12.5 μg ml^{-1}, respectively), and incubated at 37°C overnight. Standard colony PCR was performed using Vent polymerase and *attB*-PCR primers to check conjugants for presence of *catA* insert.

Expression

Large-scale expression was performed using a 15 l Chemap 3000 fermenter (AG, Switzerland). A 400 ml pre-culture of *E. coli* UM2 transformed with pET-DEST42 and conjugated with pVLT49 containing the *catA* gene was used for inoculation of 7 l of 2×LB-medium supplemented with 20 mM glucose, 100 μg ml^{-1} ampicillin, and 12.5 μg ml^{-1} chloramphenicol. The cells were grown at 30°C until OD_{600} reached about 5.0, the temperature was set to 16°C, and the cells were incubated for an hour before the expression was induced with 1 mM IPTG. Every other hour, 50 ml 20% glucose was added to the growth medium to avoid glucose starvation. A final volume of 100 ml 20% glucose was then added and the cells were harvested about 18 h after induction by centrifugation at 10,000*g* for 10 min at 4°C and stored at −20°C.

Protein purification

Cell paste from 7 l of *E. coli* UM2 culture was resuspended in extraction buffer [10 mM Tris–HCl, pH 7.5, 1 mM EDTA, 10 μM phenyl methyl sulphonyl fluoride (PMSF), and 1% (v/v) glycerol] to an OD_{600} of about 70. The cells were disrupted by sonication on ice. Pulse on/off was set to 9.9 s, temperature to 20°C, and timer to 45 min. The cell extract was centrifuged at 25,000*g* for 15 min at 4°C, and the supernatant treated with 32.5 μl 2% protamine sulphate (w/v) in extraction buffer per ml extract for 5 min with stirring at 4°C, followed by centrifugation at 25,000*g* at 4°C for 2–3 h, following filtration through glasswool.

The protein purification was performed using the Äkta FPLC Purification System and columns obtained from Amersham Pharmacia Biotech (Uppsala, Sweden). All solutions containing enzyme were always kept on ice, or at 4°C, except during the purification steps, which were performed at room temperature. The protamine sulphate fraction was diluted 1:1 with buffer A (20 mM Tris–HCl, pH 7.5) containing 10 mM NaCl and applied directly on a Q-Sepharose Fast Flow (FF) column (5.0/10) equilibrated in buffer A + 10 mM NaCl, using a flow rate of 10 ml min^{-1}. The column was washed with two column volumes (CV) buffer A + 10 mM NaCl, and the catalase enzyme was eluted with a step gradient of NaCl (0.25–0.35 M) in buffer A. Fractions of 10 ml were collected and eluates that contained the catalase were pooled.

The pooled Q-Sepharose fraction was added ammonium sulphate to 0.5 M and directly applied to a Phenyl Sepharose (High substitution) FF column (2.6/10) equilibrated in buffer A + 0.5 M ammonium sulphate, using a flow rate of 8 ml min^{-1}. The column was washed with two CV buffer A + 0.5 M ammonium sulphate, and the catalase enzyme was eluted in 10 ml fractions with a gradient of ethylene glycol (0–50%) in buffer A. Catalase containing fractions were pooled.

The Phenyl Sepharose fraction was diluted five times in buffer A and directly applied to a Source 15 Q (2.6/3.5) column equilibrated in buffer A using a flow rate of 8 ml min^{-1}. The column was washed with two CV buffer A and the enzyme was eluted in 5 ml fractions with a gradient of NaCl (0.225–0.325 M), using a flow rate of 5 ml min^{-1}. Fractions containing catalase were pooled.

Using a Vivapore 10/20 (Millipore, Billerica, MA, USA), the Source 15 Q fraction was concentrated to approximately 2.5 ml and applied to a Superdex 200 column (2.6/60) equilibrated in buffer A + 0.15 M NaCl. A flow rate of 2.5 ml min^{-1} was used, and fractions of 5 ml containing the enzyme were collected.

The pooled Superdex 200 fraction was concentrated using an Amicon Ultra-4 spin column (Millipore).

The purification of VSC is summarised in Table 2 whereas the purification table of PMC has been presented previously (Jouve et al. 1989).

Catalase activity measurements

Catalase activity was assayed using the Amplex Red Catalase Assay Kit (Molecular Probes, Eugene, OR, USA) according to the protocol supplied by the manufacturer. Briefly: the enzyme first reacts with 40 μM H_2O_2 at 22°C for 30 min, and next the Amplex Red reagent reacts with a 1:1 stoichiometry with any unreacted H_2O_2 at 37°C for 30 min in the presence of horseradish peroxidase (HRP) to produce the highly fluorescent oxidation product, Resorufin. The results are determined by subtracting the fluorescence from a no-catalase control.

Kinetic measurements of catalase activity were performed spectrophotometrically by monitoring the decrease in A_{240} resulting from the elimination of H_2O_2. ΔA_{240} min^{-1} was calculated from the initial 45 s linear portion of the curve. The ε of H_2O_2 at 240 nm was 43.6 mM^{-1} cm^{-1}.

SDS-PAGE

SDS-PAGE was performed using NuPAGE 4–12% Bis–Tris gels run in MES buffer and gels were stained with Simply Blue Safe Stain, according to the protocol supplied by the manufacturer (Invitrogen).

pH- and temperature optimum

The pH-optimum of the catalase was determined using the following10 mM buffers: sodium acetate, citric acid, MES, MOPS, Tris–HCl, diethanolamine, piperazine and glycine. The pH values were in the range from 4.0 to 10.0. All buffers were pH adjusted at 22°C. The VSC and PMC were diluted in the different buffers to 0.02–0.01 μg ml^{-1}, respectively, and each buffer was used as blank.

Temperature optimum was examined by incubation of diluted catalase in 100 mM Tris–HCl, pH 7.5 at 0, 10, 22, 30, 40, 50, 60 and 70°C, respectively, for 30 min. The pH of the buffers was adjusted at the different temperatures. H_2O_2, 40 μM, was pre-incubated at each temperature and pH-adjusted buffers used as blank for each temperature.

For pH and temperature optima, catalase activity was measured using the Amplex Red Catalase Assay Kit. Residual activity was calculated setting highest activity measured to 100%.

Temperature and pH stability measurements

The temperature and pH stability were examined by incubating diluted catalase in 10 mM MES, pH 6.5, Tris–HCl, pH 7.5 and diethanoloamine, pH 9.0, respectively, and incubations were performed at 22, 37, 50, 60 and 70°C. The pHs were adjusted at the different temperatures. Samples were collected and transferred to ice at different time intervals. The catalase dilutions (same as above) were pre-incubated for 3 min to reach the indicated temperatures before the first samples (0 min) were collected. Residual activity was measured using the Amplex Red Catalase Assay Kit. Highest activity measured was set to 100%.

Differential scanning calorimetry

Measurements were performed on a MicroCal VP-Differential scanning calorimetry (DSC) differential scanning calorimeter (MicroCal Inc., IL, USA) with cell volumes of 0.5 ml at a scan rate of 1°C min^{-1}. A 0.1 M Tris–HCl buffer, pH 7.5 was used in all experiments. Calorimetric cells were kept under an excess pressure of 30 psi to prevent degassing during the scan. Purified tetramers of VSC and PMC were used. Protein concentrations were 8.3 μM per subunit in all experiments. The thermograms were normalised for protein concentration and analysed according to a non-two-state model in order to determine the apparent T_m values and the calorimetric enthalpy (ΔH_{cal}) using the MicroCal Origin

Table 2 Purification of VSC overexpressed in *E. coli* UM2

Step	Volume (ml)	Activity (U mg^{-1})	Protein concentration (mg ml^{-1})	Total activity (U)	Total protein (mg)	Specific activity (U mg^{-1})	Yield (%)	Purification (fold)
Crude extract	360	1,298	2.14	467,107	770.4	606	100	1
Q-Sepharose	32	1,109	2.58	35,500	82.6	430	7.6	0.7
Phenyl Sepharose	40	1,677	0.30	67,078	11.9	5,627	14.4	9.3
Source 15 Q	41	377	0.12	15,457	4.8	3,222	3.3	5.3
Superdex 200	8	541	0.05	4,328	0.4	11,270	0.9	18.6

software (Version 7.0). Two DSC measurements were performed of each protein under the same conditions and both gave similar results. The denaturation of the proteins used in this experiment was found to be irreversible.

Spectroscopic measurements

A Beckman DU 640 UV-visible spectrophotometer, equipped with a cryostat, was used for light absorbance studies. Mass spectrometry measurements were performed using the MALDI-TOF (Matrix Assisted Laser Desorption Ionisation-Time of Flight) technique and a Perseptive Biosystems (Framingham, MA, USA) Voyager Elite XL time of flight mass spectrometer with delayed extraction, operating with a pulsed nitrogen laser at 337 nm. Aliquot of 0.5 µl catalase sample in 0.1 M Tris–HCl pH 7.5 buffer was mixed with 0.5 µl of a saturated solution of α-cyano-4-hydroxycinnamic acid (Sigma-Aldrich, St. Louis, MO, USA) in a 50% (v/v) solution of acetonitrile/aqueous 0.3% trifluoroacetic acid directly on the stainless steel sample plate and air-dried before analysis. The values expressed are monoisotopic mass and correspond to the $[M+H]^+$ ion.

Determination of catalase concentration, heme and protoporphyrin IX content

The concentration of tetrameric VSC was estimated spectrophotometrically using the extinction coefficient $\varepsilon_{405\ nm} = 279\ mM^{-1}\ cm^{-1}$, calculated by the formula $\varepsilon_{405} = A_{405}/c_{VSC}$. Protein concentration was determined using Bio-Rad Protein Assay Dye Reagent Concentrate based on the Bradford dye-binding procedure (Bradford 1976), according to the microtiter plate protocol described by the manufacturer (Bio-Rad, Hercules, CA, USA) using bovine serum albumine (BSA) as standard. The concentration of tetrameric PMC was estimated using the extinction coefficient $\varepsilon_{406\ nm} = 298\ mM^{-1}\ cm^{-1}$ (Andreoletti et al. 2001). The heme content was determined by the pyridine hemochromogen method (Rieske et al. 1967) by using the difference in absorbance between 556 and 580 nm measured on the redox difference spectrum where $\Delta\ (\Delta\varepsilon^{red/ox})_{556-580} = 29\ mM^{-1}\ cm^{-1}$ and expressed relative (%) to the number of monomers as explained in Andreoletti et al. (2003), using the following $\varepsilon_{280\ nm} = 79.5\ mM^{-1}\ cm^{-1}$ and $\varepsilon_{280\ nm} = 69.55\ mM^{-1}\ cm^{-1}$, for VSC and PMC monomers, respectively. Obviously the same percentages can be given for the heme saturation of the entire catalase molecule considering that all the catalase molecules are tetramers. The protoporphyrin IX content was evaluated by using the visible spectral change after the reaction of about 2–3 µM tetrameric catalase with 2 mM cyanide in 0.1 M Tris–HCl buffer pH 7.5, at room temperature, according to Andreoletti et al. (2003). The assays were performed in triplicates.

Formation of catalase complexes

Formation of catalase compound I was obtained by addition of 0.4 mM peracetic acid to native enzyme (about 1 µM tetrameric VSC) in 0.1 M Tris-maleate solution pH 7.0 at 22°C, and the optical spectrum was recorded immediately. Compound II was formed by subsequent addition of potassium ferrocyanide and ascorbate (0.1 and 9 mM final concentrations, respectively) after 8–10 min at 22°C. Contaminating hydrogen peroxide was eliminated from peracetic acid stock solutions (42 mM in Tris-maleate buffer 0.1 M, final pH 4.9) by addition of 60 nM VSC for 10 min at 4°C (Jones and Middlemiss 1972).

Fluorescence measurements of NADPH

Samples of about 2 µM tetrameric VSC were diluted in 20 mM Tris–HCl, 0.1 mM EDTA, pH 8.0. VSC was incubated 30 min at room temperature with 1.9 µM NADPH. The emission spectra (400–500 nm) of unbound or catalase-bound NADPH were measured with an Aminco Bowman Luminescence Spectrometer Serie 2, at 25°C, with an excitation wavelength set at 340 nm. In some cases, the samples were rapidly filtrated on G-50 Sephadex columns using a method of quick filtration–centrifugation (Penefsky 1977) before fluorescence measurements.

Kinetics

Measurements of catalase activity were performed by the spectrophotometric assay of catalase at 240 nm. The standard reaction mixture for the assay contained 10 mM potassium phosphate buffer (pH 7.0), with H_2O_2 concentrations ranging from 10.0 to 150 mM, and 10 µl catalase-containing solution in a total volume of 1.0 ml. The protein contents were 18.7 and 13.1 ng for VSC and PMC, respectively. K_m and k_{cat} were measured at 4, 12, 23 and 37°C, and only the initial linear rates were used to estimate the catalase activity. The amount of enzyme activity that decomposed 1 µmol of H_2O_2 per min was defined as 1 U of activity. The enzyme kinetics module in SigmaPlot (SPSS Inc., Chicago, IL, USA) was used for calculations of the kinetic constants. The observed kinetic constants (k_{cat}/K_m) were corrected for heme content in VSC and PMC, and the values were calculated per heme saturated tetrameric molecule.

Nucleotide sequence accession number

The sequence of the *V. salmonicida* LFI1238 catalase gene has been submitted to GenBank database under accession no. DQ182487.

Results

Gene identification

The sequence of the PCR-product generated from genomic DNA of *V. salmonicida* LFI1238 as template was identified as catalase, and primers were designed for primer-walking experiments on the BAC-clone in order to obtain the full-length sequence of the gene (accession no. DQ182487). The *catA* protein coding sequence (CDS) encodes a protein of 483 amino acids initiated with an atg codon and terminated with a stop (taa) codon at nucleotide 1450. The monomer molecular mass was predicted to 54,741 Da and a pI of 5.92. A potential Shine–Dalgarno (SD) sequence or ribosome-binding site was identified at positions -13 to -5 upstream of the atg initiation codon. The putative -35 and -10 promoter areas were identified at positions -47 to -42 and -32 to -19, respectively, upstream of the potential SD sequence. An analysis of the upstream sequence of the gene (-10 region) revealed a potential σ^S binding site. The predicted binding site is similar to the $TGN_{(0-2)}CYANNNMT$ (Lacour and Landini 2004) consensus sequence recently proposed for σ_S. However, our matrix (from 150 experimentally validated σ^S promoter sequences, unpublished results) indicates that the site is extended with three more bases downstream of the −7 T nucleotide. A putative base-paired hairpin termination signal was found approximately 33–63 nucleotides downstream of the stop codon.

Alignment

Vibrio salmonicida catalase and PMC consist of 483 and 484 amino acids, respectively (Fig. 1). The identity between VSC and PMC is 71% while the similarity is 83%. There are 139 amino acid substitutions between VSC and PMC, and 75 and 76 are in unique positions for VSC and PMC, whereas 63 amino acids share the same properties. The unique substitutions in VSC are mainly localised in the α-helical domain (residues 417–484, PMC numbering) in the C-terminal part of the sequence, where the identity to PMC is about 45%. In the N-terminal arm (residues 1–55), the β-barrel domain (residues 56–301), and in the wrapping domain (residues 302–416), the identity is approximately 90% to PMC. However, a major part of the substitutions in the β-barrel domain and in the wrapping domain are found in the C-terminal parts of these regions. Residues suggested being involved in catalysis and cofactor binding are highly conserved.

Expression and purification of *Vibrio salmonicida* catalase

The *catA* gene from *V. salmonicida* was subcloned into the plasmid pET-DEST42 for expression. *E. coli* UM2, a *catE*/*catG*-deficient strain, was transformed with this construct and a positive transformant was identified and used for small-scale expression testing.

Different temperatures for expression were tested. At temperatures above 25°C, the VSC was insoluble while expression at 20, 18 and 16°C produced soluble protein. The activity was slightly higher at 16°C, and this temperature was therefore used for large-scale expression.

Expression of VSC was performed in 7 l batch fermentation, and 25 mg of recombinant VSC with a molecular weight of 57 kDa was purified to apparent homogeneity as determined by SDS-PAGE. The tetrameric molecular weight was estimated by gel filtration to 235 kDa, which is in agreement with the corresponding monomer of 57 kDa. The specific activity of VSC at 37°C was determined to $195{,}000 \pm 10{,}000$ U mg^{-1}, using the standard spectrophotometric method with 60 mM H_2O_2 concentration. Initial purification experiments were performed according to the His-tag purification protocol, but the protein did not bind to the matrix. The C-terminal His-tags are probably buried in the structure and thus not able to bind to the nickel-affinity column. An alternative procedure including ion exchange, hydrophobic affinity, and gel filtration was thus developed as described in experimental procedures. As shown in Table 2, the four-step procedure achieved an 18.6-fold purification over crude extract and a yield of 0.9%.

Temperature and pH effect on VSC compared to PMC

In order to define the pH optimum profile for VSC activity, the enzyme was incubated for 30 min in different buffers ranging from pH 4.0 to 10.0. The optimal pH for activity of VSC was defined in diethanolamine buffer at an approximate pH of 8.8 with a distinct peak (results not shown), but a wide plateau of residual activity (about 50%) was observed from pH 6.0 to 9.5. In these experimental conditions, PMC also presented a plateau in this pH range, as previously reported (Jouve et al. 1983b).

The temperature optimum for activity of VSC and PMC was determined by incubating the enzymes in a Tris–HCl buffer of pH 7.5 ranging from 0 to 70°C as shown in Fig. 2. Optimal temperature for VSC activity was measured between 0 and 10°C while PMC showed a broader optimum from approximately 20 to 50°C.

The thermostability of VSC and PMC was determined at 37, 50 and 60°C, and at 70°C for PMC, in 10 mM diethanolamine, pH 9.0 as illustrated in Fig. 3. Half-lives of VSC and PMC were estimated from the curves in Fig. 3. The results show high stability at 37°C, with half-lives of 6.5 and 13.5 h of VSC and PMC, respectively. At 50°C, the half-life of VSC is approximately 34 min, while the half-life of PMC is more than six times higher (> 180 min). Increasing the temperature to 60°C has drastic impact on the stability of VSC and shows a half-life of less than 5 min, while

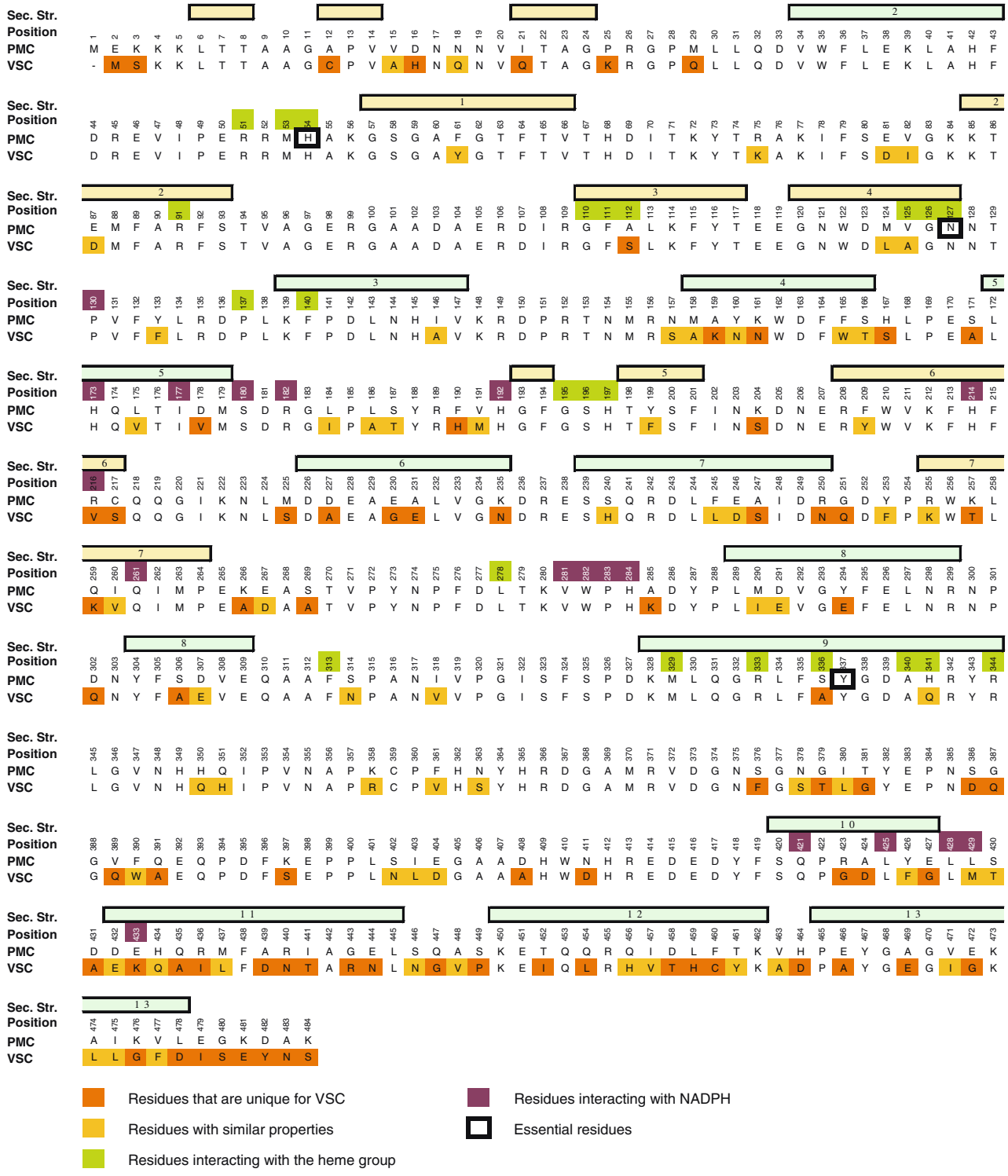

Fig. 1 Sequence alignment of VSC and PMC. Comparison of the deduced amino acid sequences of VSC and PMC. The amino acids are given in *single-letter code*. Secondary structure and position from PMC (PDB entry 1M85) are shown above the sequences. The naming of the secondary structure elements are based on the PDB entry file of PMC, which again are based on the BLC 3D structure (Fita et al. 1986). Small strands at the N-terminal of the structure are defined in the PDB-file but not named. *Pale yellow*, strands; *pale green*, helices; *orange*, residues that are unique for VSC; *gold*, residues with similar properties; *green*, residues that are interacting with the heme group; *purple*, residues that are interacting with NADPH; *bold box*, residues that are essential in the active site (Gouet et al. 1995). The N-terminal arm consists of the first 55 residues, residues 56–301 constitute the barrel domain, residues 302–416 the wrapping domain, and the C-terminal 417–484 residues constitute the helical domain (Gouet et al. 1995)

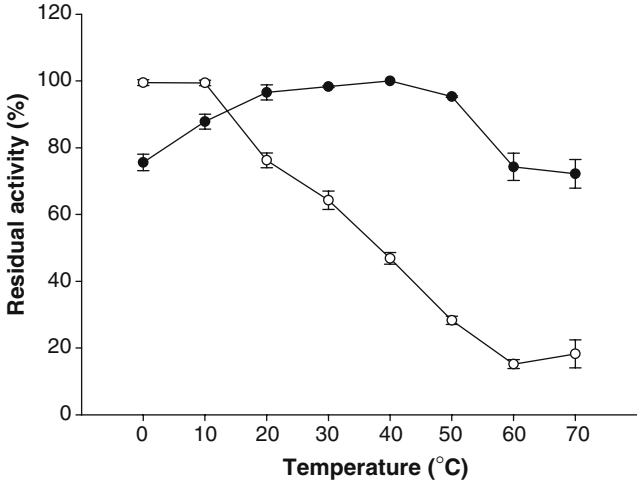

Fig. 2 Temperature optimum profile for VSC and PMC activity. Enzymes and substrate were incubated at temperatures from 0 to 70°C for 30 min and residual catalase activity was measured using the Amplex Red Catalase Assay Kit. Highest residual activity measured was set to 100%. Temperature optimum for VSC obtained at approximately 0–10°C and for PMC a broad optimum ranging from approximately 20–50°C. *open circle*, residual VSC activity; *closed circle*, residual PMC activity

the stability of PMC is still moderate with a half-life of approximately 50 min. At 70°C VSC was totally inactivated, and the stability of PMC was reduced considerably showing a half-life of about 15 min. The thermostability experiments were also performed with 10 mM MES buffer, pH 6.5, and 10 mM Tris–HCl, pH 7.5, with similar results as described above. The thermal stability of PMC have previously been determined at 68.5°C with a half-live of 12 min, in agreement with these results (approximately 15 min at 70°C), considering the margin of error due to the difference of methodology (Jouve et al. 1983a). Both VSC and PMC showed the same trends in half-life at pH 6.5 and 7.5 (results not shown), indicating that pH does not have any impact on thermostability in this pH range.

The thermal stability and calorimetric enthalpy of VSC and PMC was further investigated using microcalorimetry. The normalised curves showed single peaks and gave apparent T_m of 59 and 78°C and calorimetric enthalpy (ΔH_{cal}) on approximately 246 and 278 kcal mol^{-1} of VSC and PMC, respectively (Fig. 4, and Table 3).

UV-visible spectral characterisation of VSC and its prosthetic group

The visible absorption spectrum of VSC presented major peaks at 278 and 405 nm (Soret band) and three minor peaks at 511, 548 and 630 nm (Fig. 5, solid line), with a Rz (A_{405}/A_{280}) index of 1.0. This spectrum was similar to the PMC spectrum (Jouve et al. 1983b). However, an additional peak for VSC observed at 574 nm, a slight red-shift of the bands in the 500–540 nm region, and the narrow form of the charge transfer band at 630 nm were unusual and reminiscent of the results obtained for recombinant PMC (Andreoletti et al. 2003). These peaks indicated the presence of protoporphyrin IX. The analysis of the prosthetic group in VSC performed by MALDI mass spectrometry showed two peaks of 563 and 616 Da, corresponding to protoporphyrin IX and heme *b*, respectively (Fig. 6).

The reaction with cyanide is characterised by a red shift of the Soret band towards 420 nm with a shoulder near 350–360 nm and the disappearance of the bands in the 500–700 nm region, replaced by a peak at 550 nm with a shoulder at about 590 nm (Jouve et al. 1984). These modifications were observed in the spectrum of the VSC cyanide complex, but two other peaks, at 514 and 630 nm (Fig. 5, dotted line), indicated the presence of protoporphyrin IX, which could not participate in the formation of the cyanide derivative. The remaining absorbance at 630 nm, after the cyanide reaction, allowed estimation of the protoporphyrin IX content of VSC to 25% (Andreoletti et al. 2003). The spectral changes produced by the reaction of VSC with peracetic acid to form compound I, and compound II after a subsequent addition of ascorbate plus ferrocyanide, were shown on the difference spectra (compound I minus native, Fig. 7a; compound II minus native, Fig. 7b) of the two compounds. They were quite similar to those obtained for PMC (Andreoletti et al. 2003; Jouve et al. 1989) and indicated that the presence of protoporphyrin IX did not interfere with the reaction.

The nature of heme *b* was confirmed by the visible spectrum of the pyridine ferro-hemochrome of VSC with major absorbance bands at 418, 524 and 556 nm (Falk 1964). The heme content was determined to 67% (see Materials and methods). The complement (8%) to 100% from the sum of heme and protoporphyrin IX could be explained by the presence of damaged heme which cannot be counted in the cyanide assay, as previously described for PMC (Andreoletti et al. 2003).

VSC binding of NADPH: fluorescence

Native purified VSC did not present any peak of fluorescence emission when excited at the wavelength (340 nm) (Fig. 8, trace 1), showing the absence of detectable NADPH in our VSC preparation. The addition of sub-stoichiometric concentration of NADPH (a quarter of VSC monomer concentration) resulted in an emission spectrum with a maximum at 444 nm (Fig. 8, trace 3), different from the maximum obtained for NADPH without protein (460 nm) (Fig. 8, trace 5). The fluorescence emission intensity of free NADPH was also higher than in the mixture with the protein, showing that the fluorescence was partly quenched by the presence of VSC. The filtration of NADPH-containing VSC sample on G-50 Sephadex

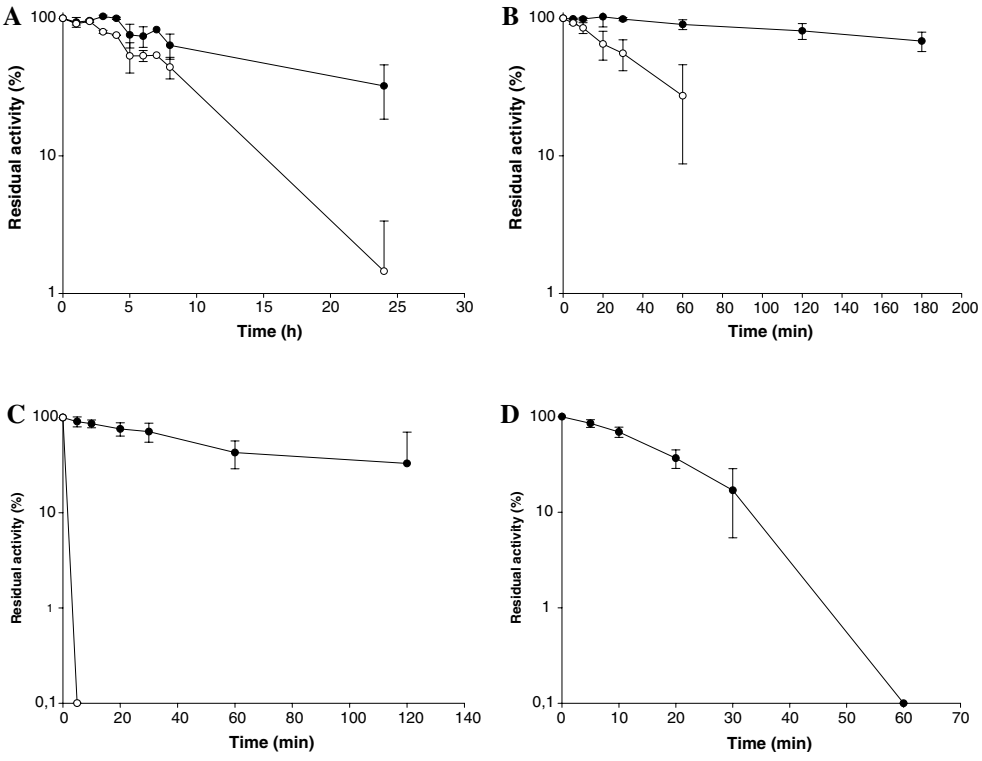

Fig. 3 Temperature stability of VSC and PMC. Enzymes were initially pre-incubated for 3 min at four different temperatures, A, 37; B, 50; C, 60; and D, 70°C (only PMC) and residual activity measurements set to 100%. Aliquots were taken after different time intervals and residual activity was measured using the Amplex Red Catalase Assay kit. *open circle*, residual VSC activity; *closed circle*, residual PMC activity

did not change the emission spectrum (Fig. 8, trace 4). In contrast, free NADPH was totally retained on a G-50 Sephadex column (Fig. 8, trace 2).

Kinetic properties of VSC and PMC

The apparent kinetic constants for VSC and PMC, K_m and k_{cat}, were determined at four different temperatures with H_2O_2 concentrations ranging from 10 to 150 mM. At these conditions, all small-subunit catalases follow the Michaelis–Menten-like kinetics, and the V_{max} and K_m values are reliable (Switala and Loewen 2002), even though the theoretical values of V_{max}, and thus k_{cat}, can be higher than observed due to catalase inactivation at elevated H_2O_2 concentrations (Lardinois et al. 1996). To take into account the variation of heme saturation (see Materials and methods) in VSC and PMC (67 and 75%, respectively), k_{cat} was calculated per heme saturated catalase tetramer. The differences in apparent K_m, k_{cat} and k_{cat}/K_m are shown in Table 4. K_m was generally lower (between 1.2 and 1.6 times) for VSC than PMC at all temperatures measured. At 4°C the k_{cat} for VSC was about 1.3 times higher than for PMC, whereas the opposite result was seen at 12 and 37°C. Both enzymes shared the same turnover number at 23°C. The catalytic efficiency, k_{cat}/K_m, was approximately twofold higher for VSC at 4°C and approximately 1.2-fold higher at 12, 23 and 37°C compared to PMC.

The K_m increased with increasing temperature for both enzymes. The results revealed an increase in k_{cat} for VSC with temperature, except at 37°C where k_{cat} was slightly decreased. k_{cat} for PMC was increasing throughout the measured temperature range. k_{cat}/K_m for VSC remained constant below 12°C, whereas it decreased sharply for PMC. From 23 to 12°C, k_{cat}/K_m decreased with decreasing temperature for VSC and PMC, and from 37 to 23°C it increased with increasing temperature.

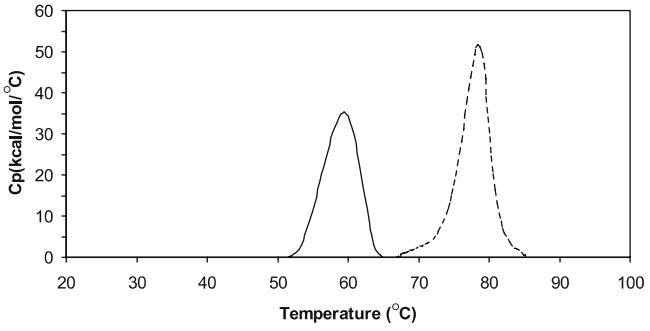

Fig. 4 Thermal unfolding of VSC and PMC. Unfolding as monitored by DSC at a scan rate of 1°C min^{-1}. VSC (*continuous line*) and PMC (*dashed line*). Both thermograms are baseline subtracted and normalised for protein concentrations

Table 3 Apparent T_m and ΔH of VSC and PMC

Protein	T_m (°C)	ΔH (kcal mol^{-1})
VSC	59.07 ± 0.047	246.1 ± 3.96
PMC	77.68 ± 0.035	276.6 ± 3.83

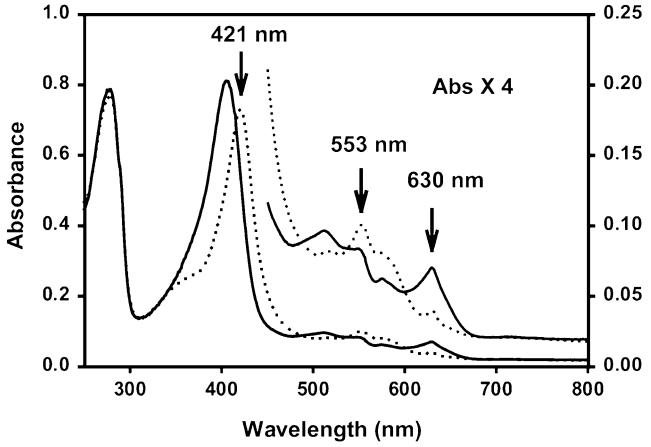

Fig. 5 UV-visible spectra of native VSC and cyanide derivative. The absorption spectrum of 2.5 μM tetrameric native VSC was measured at room temperature in 0.1 M Tris–HCl buffer pH 7.5 (*solid line*). The cyanide derivative was obtained by addition of 2 mM KCN to the native VSC sample. The spectrum was immediately recorded at room temperature (*dotted line*) and no further change was observed with time; on the right side of the graph, a fourfold expansion of the 450–800 nm region

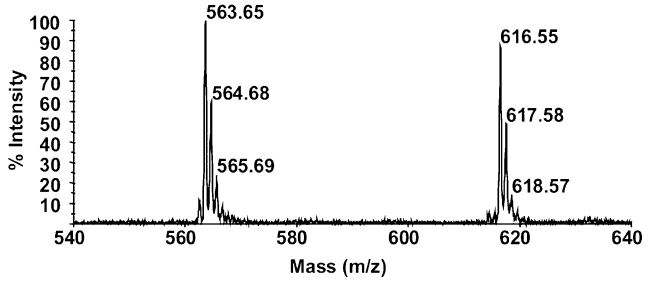

Fig. 6 MALDI analysis of the prosthetic group of VSC. Catalase samples (0.5 μL) in 0.1 M Tris–HCl pH 7.5 buffer was mixed with an equal volume of a saturated solution of cyano-4-hydroxycinnamic acid (Sigma) in a 50% (v/v) solution of acetonitrile/aqueous 0.3% trifluoroacetic acid directly on the stainless steel sample plate and air-dried before analysis. The values expressed are monoisotopic mass and correspond to the $[M+H]^+$ ion. The theoretical masses of protoporphyrin IX and heme are 563 and 616 Da, respectively

Discussion

Catalases are enzymes with high specific activity (k_{cat}) where the reaction occurs immediately after the protein and substrate encounter each another. They display a low Q_{10} value (Hochachka 1991) and are said to be nearly diffusion controlled (Fersht 1985). In this study, we characterised the recombinant catalase from the psychrophilic marine bacterium *V. salmonicida* strain LFI1238 (VSC) and compared it to the mesophilic *P. mirabilis* monofunctional heme-containing catalase (PMC) in order to determine possible cold adapted features of VSC. PMC was chosen as a mesophilic counterpart of VSC due to the high sequence homology, the solved structure and the availability of the enzyme.

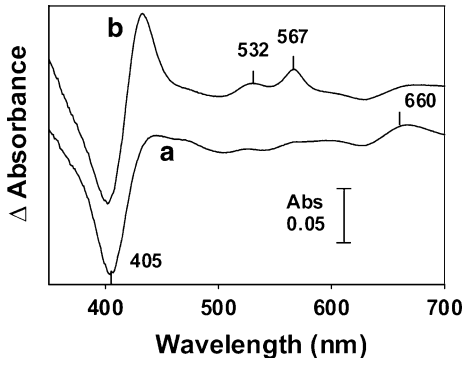

Fig. 7 Difference spectra between VSC compound I, II and the native state. Compound I was obtained by addition of 0.4 mM peracetic acid, free of contaminating hydrogen peroxide (see Experimental procedures), to about 1 μM tetrameric VSC in 0.1 M Tris-maleate buffer pH 7 at 22°C, and the visible spectrum was recorded immediately. Compound II was obtained by subsequent addition of 0.1 mM potassium ferrocyanide and 9 mM ascorbate after 8 min at 22°C. **a** compound I minus native state enzyme; **b** compound II minus native state enzyme

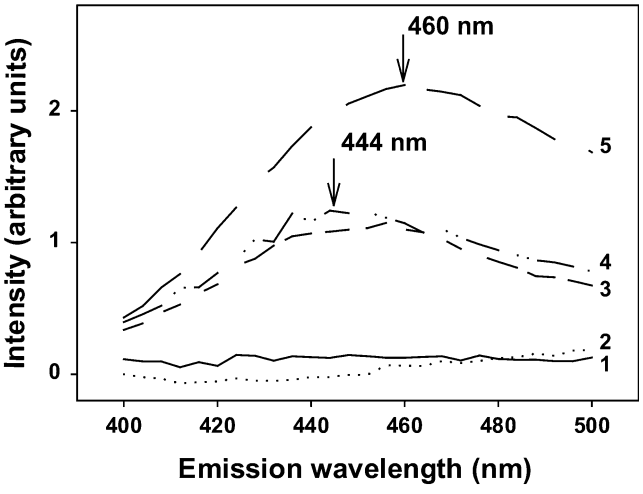

Fig. 8 Effect of NADPH on the VSC fluorescence emission spectrum. Fluorescence emission spectra of VSC after substraction of background buffer emission signal. Excitation wavelength set at 340 nm. (1) 2.6 μM tetrameric VSC, 20 mM Tris–HCl, 0.1 mM EDTA, pH 8; (2) G-50 Sephadex filtrated (see Experimental procedures) 1.9 μM NADPH, 20 mM Tris–HCl, 0.1 mM EDTA, pH 8; (3) 2.6 μM tetrameric VSC, 20 mM Tris–HCl, 0.1 mM EDTA, pH 8, incubated with 1.9 μM NADPH 30 min at room temperature; (4) G-50 Sephadex filtrated 2.6 μM tetrameric VSC, 1.9 μM NADPH, 20 mM Tris–HCl, 0.1 mM EDTA, pH 8; (5) 1.9 μM NADPH, 20 mM Tris–HCl, 0.1 mM EDTA, pH 8

Catalase from *V. salmonicida* was expressed in *E. coli* UM2 at low temperature to obtain high degree of soluble protein, and purified to apparent homogeneity. As seen from the data in Table 2, the low yield of purified VSC is characterised by a high specific activity. The molecular weight of monomeric VSC was determined to 57 kDa and the tetrameric form of the enzyme to 235 kDa. These results correlate with the purification of

Table 4 Kinetic apparent constants determined for VSC and PMC

Catalase	T (°C)	V_{max} (U mg^{-1})	k^{a}_{cat} (s^{-1})	K_m (mM)	k^{a}_{cat}/K_m (s^{-1} M^{-1})
VSC	4	$2.32\times10^5 \pm 67{,}800$	1.36×10^6	51.1 ± 3.5	2.67×10^7
	12	$2.77\times10^5 \pm 75{,}000$	1.64×10^6	61.6 ± 6.5	2.65×10^7
	23	$5.75\times10^5 \pm 46{,}000$	3.35×10^6	103.6 ± 12.7	3.23×10^7
	37	$5.68\times10^5 \pm 77{,}400$	3.33×10^6	118.4 ± 18.2	2.82×10^7
PMC	4	$2.17\times10^5 \pm 74{,}200$	1.08×10^6	82.7 ± 2.2	1.30×10^7
	12	$4.04\times10^5 \pm 108{,}900$	2.00×10^6	88.3 ± 9.2	2.27×10^7
	23	$6.74\times10^5 \pm 32{,}100$	3.33×10^6	127.0 ± 7.5	2.62×10^7
	37	$9.05\times10^5 \pm 31{,}100$	4.48×10^6	189.4 ± 13.4	2.37×10^7

[a]Considering that the heme saturation (see Materials and methods) of VSC and PMC was different (67 and 75%, respectively) and in order to obtain the best comparison of data, the experimental k_{cat} values were corrected to obtain the results for an ideal tetrameric molecule fully saturated in heme

other monofunctional catalases isolated from prokaryotic and eukaryotic organisms having molecular weights in the range of 200–340 kDa and containing four equally sized subunits each with a prosthetic heme group (Maté et al. 1999).

The visible spectrum of VSC, with a Soret peak at 405 nm, and weaker bands at 511 nm (with a shoulder at 548 nm) and at 630 nm is typical of ferric protoheme proteins such as catalases (Nicholls et al. 2001). However, protoporphyrin IX, identified by spectrophotometry and mass spectroscopy, is also present in non-negligible proportions (25%) in our VSC preparation, as already mentioned in the recombinant form of PMC (Andreoletti et al. 2003). The content of heme *b* in VSC was estimated to 67%. The remaining 8% could be the result of in situ heme degradation, as mentioned for PMC and other catalases (Gouet et al. 1995). Protoporphyrin IX does not disturb the functioning of VSC, as demonstrated by the formation of cyanide complex and compounds I and II, similar to other monofunctional heme catalases (Andreoletti et al. 2003). The presence of protoporphyrin IX could be a result of a too rapid synthesis of apocatalase compared to the heme biosynthesis, or a too weak iron concentration or incorporation in the heme in the *E. coli* expression system. Future expression of VSC should therefore be carried out with addition of exogenous heme in order to increase the heme content of the enzyme. Protoporphyrin IX incorporation has already been observed in another recombinant form of PMC without alteration of its 3D structure (Andreoletti et al. 2003). The binding of a prosthetic group without iron must lead to a less solid structure than when heme is bound. If a high flexibility generally characterises the structure of psychrophilic enzymes, and the amino acid sequence of VSC suggests that it has this particularity (Riise et al. 2006), this psychrophilic character does not impede VSC to incorporate protoporphyrin IX in place of heme.

Purified VSC does not contain NADPH but is able to bind the co-factor. This is shown by the change in the fluorescence emission maximum of NADPH spectrum (460–444 nm) in presence of VSC, as reported for several other NADPH binding catalases (Hillar et al. 1994). The affinity could be sufficiently high (K_d of micromolar range or less) to avoid the release of NADPH after a rapid filtration–centrifugation on G-50 Sephadex gel. It is not surprising that VSC can bind NADPH because all the amino acid residues involved in the NADPH binding of PMC are conserved in VSC sequence, except of PMC Arg216 and Glu433 replaced by Val and Lys, respectively. However, it is possible that these two changes may affect the reactivity of VSC with the co-factor.

The specific activity of VSC was determined to $195{,}000 \pm 10{,}000$ U mg^{-1} at 37°C in 60 mM H_2O_2, and was similar to that of PMC ($222{,}000 \pm 11{,}000$ U mg^{-1}) determined under the same conditions and is in agreement with the specific activity of PMC (160,000 U mg^{-1}) published by Switala and Loewen (2002).

Vibrio salmonicida catalase showed a broad pH activity range (from pH 6 to 9.5) as previously reported for PMC or other monofunctional catalases characterised, whereas the catalase-peroxidases do not possess this feature (Nicholls et al. 2001).

Optimal temperature for activity of VSC (0–10°C) was found to be much lower than for the mesophilic PMC (20–50°C). At temperatures below 10°C, the residual activity was higher for VSC than PMC. At temperatures higher than 20°C, VSC showed a lower residual activity than PMC, presumably as a consequence of the low thermostability of VSC.

Temperature stability experiments revealed that VSC was more temperature labile than PMC at all temperatures tested. At 60°C, VSC had a half-life of less than 5 min compared to 50 min for PMC, whereas the corresponding half-lives at 50°C were 30 min of VSC and more than 180 min of PMC. At lower temperatures, the difference in half-life was less pronounced, even though PMC always remained more thermostable than VSC. The thermal stability of the wild-type (WT) and the regulation mutant (PR) catalase from *P. mirabilis* has previously been determined at 68.5 and 75°C (Jouve et al. 1983a). Half-lives of the WT and PR catalase at 68.5°C were approximately 5 and 12 min, respectively. The half-life of cold adapted proteins is described as significantly reduced at elevated temperatures compared to the mesophilic and thermophilic counterparts, and in most cases found to be in the order of 7–10 min at 45–

55°C (Smalas et al. 2000), similar to the results presented therein.

Microcalorimetric measurements were performed to investigate the temperature stability and the calorimetric enthalpy for unfolding of VSC and PMC. The result shows that the melting temperature of VSC is approximately 20°C lower than for PMC (Fig. 4, Table 3), and supports the previous stability measurements in presence of substrate (Fig. 3). The calorimetric analysis further showed a lower calorimetric enthalpy for unfolding of VSC compared to PMC. Both these results are in agreement with similar analysis of other cold adapted proteins, e.g. α-amylases (D'Amico et al. 2003), xylanases (Collins et al. 2003) and DNA ligases (Georlette et al. 2003).

The apparent catalytic efficiency, k_{cat}/K_m, per heme saturated tetrameric molecule in VSC was found to be higher than in PMC at all temperatures measured. The catalytic efficiency of VSC remained almost constant between 4 and 12°C, while the one for PMC increased sharply. Apparent K_m and k_{cat} increased between 4 and 37°C for both enzymes. However K_m always remained inferior for VSC compared to PMC, while k_{cat} of VSC was higher than k_{cat} of PMC at low temperatures (4–12°C). At high temperatures (23–37°C), K_m and k_{cat} of VSC levelled off, whereas the same constants increased in PMC. To summarise, our kinetics and stability measurements showed that VSC possessed the typical cold adapted features as reduced thermostability and increased catalytic efficiency compared to its mesophilic counterpart PMC.

Catalases are often regarded as perfectly evolved where the reaction rate is diffusion-controlled and essentially temperature independent (Georlette et al. 2003). As a consequence, catalases should not exhibit any drastic kinetic adaptation at low temperatures. However, our result not only shows that the VSC is more efficient at all temperatures compared to PMC, but the catalytic efficiency of VSC and PMC is almost temperature independent, except at 4°C where PMC has a twofold lower efficiency. This may indicate that VSC has evolved to maintain a high efficiency at low temperatures compared to PMC. Psychrophiles display metabolic fluxes at low temperatures that are basically comparable to those exhibited by closely related mesophiles living at moderate temperatures. Since catalases are essential for degradation of hydrogen peroxide to prevent oxidative damage, high-catalytic efficiency is required.

In monofunctional catalases, the substrate (H_2O_2) must gain access to the deeply buried heme-active site through a long channel (main channel). In *E. coli* HPII, it has been demonstrated that substituting a negatively charged side chain in the main channel by smaller, larger or polar side chains reduces the activity up to 90% (Chelikani et al. 2003). The authors conclude that volume and shape of the main channel together with electrostatic effects may influence the optimum substrate access. It is reasonable to propose that VSC may have evolved a more optimised main channel for substrate access and catalysis at low-temperature compared to PMC.

Based on structure modelling and crystallographic data, Georlette et al. (2004) concluded in a recent review that each psychrophilic enzyme adopts its own strategy and that there is a continuum in the strategy of protein adaptations to temperature. Some of the characterised strategies include reduced number of salt bridges, hydrogen bonds, aromatic—aromatic interactions, proline, and arginine residues, as well as larger loops and greater exposure of non-polar groups to solvent (Feller et al. 1997). Homology modelling, crystallisation, and structural determination of the VSC are ongoing and required in order to get more insight into the high catalytic efficiency of this diffusion-controlled enzyme.

Acknowledgements This work was supported by The Norwegian Research Council grant 143450/140 and partly by the national Functional Genomics Programme (FUGE) in The Research Council of Norway. We gratefully acknowledge Jonas Jakobsen at the Department of Molecular Biotechnology, Institute of Medical Biology, University of Tromsø, Norway, for technical assistance; Dr. Sigrun Espelid, NorStruct, Department of Chemistry, University of Tromsø, Norway for reading of the manuscript; and Dr. Bernard Dublet of the Institute of Stuctural Biology (IBS), Grenoble, France for the MALDI mass spectroscopy measurements.

References

Andreoletti P, Gambarelli S, Sainz G, Stojanoff V, White C, Desfonds G, Gagnon J, Gaillard J, Jouve HM (2001) Formation of a tyrosyl radical intermediate in *Proteus mirabilis* catalase by directed mutagenesis and consequences for nucleotide reactivity. Biochemistry 40:13734–13743

Andreoletti P, Sainz G, Jaquinod M, Gagnon J, Jouve HM (2003) High-resolution structure and biochemical properties of a recombinant *Proteus mirabilis* catalase depleted in iron. Proteins 50:261–271

Ardissone S, Frendo P, Laurenti E, Jantschko W, Obinger C, Puppo A, Ferrari RP (2004) Purification and physical-chemical characterization of the three hydroperoxidases from the symbiotic bacterium *Sinorhizobium meliloti*. Biochemistry 43:12692–12699

Bradford MM (1976) A rapid and sensitive method for the quantitation of microgram quantities of protein utilizing the principle of protein-dye binding. Anal Biochem 72:248–254

Bravo J, Verdaguer N, Tormo J, Betzel C, Switala J, Loewen PC, Fita I (1995) Crystal structure of catalase HPII from *Escherichia coli*. Structure 3:491–502

Cabiscol E, Tamarit J, Ros J (2000) Oxidative stress in bacteria and protein damage by reactive oxygen species. Int Microbiol 3:3–8

Carpena X, Soriano M, Klotz MG, Duckworth HW, Donald LJ, Melik-Adamyan W, Fita I, Loewen PC (2003) Structure of the Clade 1 catalase, CatF of *Pseudomonas syringae*, at 1.8 A resolution. Proteins 50:423–436

Chelikani P, Carpena X, Fita I, Loewen PC (2003) An electrical potential in the access channel of catalases enhances catalysis. J Biol Chem 278:31290–31296

Collins T, Meuwis MA, Gerday C, Feller G (2003) Activity, stability and flexibility in Glycosidases adapted to extreme thermal environments. J Mol Biol 328:419–428

D'Amico S, Gerday C, Feller G (2003) Temperature adaptation of proteins: engineering mesophilic-like activity and stability in a cold-adapted alpha-amylase. J Mol Biol 332:981–988

Falk JE (1964) Porphyrins and metalloporphyrins, vol 2. BBA Library, Elsevier, New York
Feller G, Gerday C (1997) Psychrophilic enzymes: molecular basis of cold adaptation. Cell Mol Life Sci 53:830–841
Fersht A (1985) Upper limits on rate constants. In: Fersht A (eds) Enzyme structure and mechanism. 2nd edn. W H Freeman and company, New York, pp 147–149
Figurski DH, Helinski DR (1979) Replication of an origin-containing derivative of plasmid RK2 dependent on a plasmid function provided in trans. Proc Natl Acad Sci USA 76:1648–1652
Fita I, Silva AM, Murthy MR, Rossmann MG (1986) The refined structure of beef liver catalase at 2.5 Å resolution. Acta Crystallogr B 42:497–515
Fridovich I (1978) The biology of oxygen radicals. Science 201:875–880
Georlette D, Damien B, Blaise V, Depiereux E, Uversky VN, Gerday C, Feller G (2003) Structural and functional adaptations to extreme temperatures in psychrophilic, mesophilic, and thermophilic DNA ligases. J Biol Chem 278:37015–37023
Gouet P, Jouve HM, Dideberg O (1995) Crystal structure of *Proteus mirabilis* PR catalase with and without bound NADPH. J Mol Biol 249:933–954
Grant SGN, Jessee J, Bloom FR, Hanahan D (1990) Differential plasmid rescue from transgenic mouse DNAs into *Escherichia coli* methylation-restriction mutants. Proc Natl Acad Sci USA 87:4645–4649
Hakansson KO, Brugna M, Tasse L (2004) The three-dimensional structure of catalase from *Enterococcus faecalis*. Acta Crystallogr D 60:1374–1380
Hall TA (1999) BioEdit: a user-friendly biological sequence alignment editor and analysis program for Windows 95/98/NT. Nucleic Acids Symp Ser 41:95–98
Hassett DJ, Cohen MS (1989) Bacterial adaptation to oxidative stress: implications for pathogenesis and interaction with phagocytic cells. FASEB J 3:2574–2582
Herrero M, de Lorenzo V, Ensley B, Timmis KN (1993) A T7 RNA polymerase-based system for the construction of *Pseudomonas* strains with phenotypes dependent on TOL-meta pathway effectors. Gene 134:103–106
Herrero M, de Lorenzo V, Timmis KN (1990) Transposon vectors containing non-antibiotic resistance selection markers for cloning and stable chromosomal insertion of foreign genes in gram-negative bacteria. J Bacteriol 172:6557–6567
Hillar A, Nicholls P, Switala J, Loewen PC (1994) NADPH binding and control of catalase compound II formation: comparison of bovine, yeast, and *Escherichia coli* enzymes. Biochem J 300(Pt 2):531–539
Hochachka PW (1991) Temperature: the ectothermy options. In: Hochachka, Mommsen (eds) Biochemistry and molecular biology of fishes, vol 1. Elsevier Science Publishers B V, Amsterdam, pp313–322
Jones P, Middlemiss DN (1972) Formation of compound I by the reaction of catalase with peroxoacetic acid. Biochem J 130:411–415
Jouve HM, Beaumont F, Léger I, Foray J, Pelmont J (1989) Tightly bound NADPH in *Proteus mirabilis* PR catalase. Biochem Cell Biol 67:271–277
Jouve HM, Gaillard J, Pelmont J (1984) Characterization and spectral properties of *Proteus mirabilis* PR catalase. Can J Biochem Cell Biol 62:935–944
Jouve HM, Lasauniere C, Pelmont J (1983a) Properties of a catalase from a peroxide-resistant mutant of *Proteus mirabilis*. Can J Biochem Cell Biol 61:1219–1227
Jouve HM, Tessier S, Pelmont J (1983b) Purification and properties of the *Proteus mirabilis* catalase. Can J Biochem Cell Biol 61:8–14
Lacour S, Landini P (2004) SigmaS-dependent gene expression at the onset of stationary phase in *Escherichia coli*: function of sigmaS-dependent genes and identification of their promoter sequences. J Bacteriol 186:7186–7195
Lardinois OM, Mestdagh MM, Rouxhet PG (1996) Reversible inhibition and irreversible inactivation of catalase in presence of hydrogen peroxide. Biochim Biophys Acta 1295:222–238
Loewen PC, Carpena X, Rovira C, Ivancich A, Perez-Luque R, Haas R, Odenbreit S, Nicholls P, Fita I (2004) Structure of *Helicobacter pylori* catalase, with and without formic acid bound, at 1.6 Å resolution. Biochemistry 43:3089–3103
Loewen PC, Switala J (1986) Purification and characterization of catalase HPII from *Escherichia coli* K12. Biochem Cell Biol 64:638–646
Maté MJ, Zamocky M, Nykyri LM, Herzog C, Alzari PM, Betzel C, Koller F, Fita I (1999) Structure of catalase-A from *Saccharomyces cerevisiae*. J Mol Biol 286:135–149
Murshudov GN, Grebenko AI, Brannigan JA, Antson AA, Barynin VV, Dodson GG, Dauter Z, Wilson KS, Melik-Adamyan WR (2002) The structures of *Micrococcus lysodeikticus* catalase, its ferryl intermediate (compound II) and NADPH complex. Acta Crystallogr D 58:1972–1982
Murshudov GN, Melik-Adamyan WR, Grebenko AI, Barynin VV, Vagin AA, Vainshtein BK, Dauter Z, Wilson KS (1992) Three-dimensional structure of catalase from *Micrococcus lysodeikticus* at 1.5 A resolution. FEBS Lett 312:127–131
Nicholls P, Fita I, Loewen PC (2001) Enzymology and structure of catalases. Adv Inorg Chem 51:51–106
Penefsky HS (1977) Reversible binding of Pi by beef heart mitochondrial adenosine triphosphatase. J Biol Chem 252:2891–2899
Rieske JS, Baum H, Stoner CD, Lipton SH (1967) On the antimycin-sensitive cleavage of complex 3 of the mitochondrial respiratory chain. J Biol Chem 242:4854–4866
Riise EK, Lorentzen MS, Helland R, Willassen NP (2006) Crystallization and preliminary X-ray diffraction analysis of a cold-adapted catalase from *Vibrio salmonicida*. Acta Crystallogr F 62:77–79
Smalas AO, Leiros HK, Os V, Willassen NP (2000) Cold adapted enzymes. Biotechnol Annu Rev 6:1–57
Switala J, Loewen PC (2002) Diversity of properties among catalases. Arch Biochem Biophys 401:145–154
Thompson JD, Plewniak F, Thierry J, Poch O (2000) DbClustal: rapid and reliable global multiple alignments of protein sequences detected by database searches. Nucleic Acids Res 28:2919–2926
Visick KL, Ruby EG (1998) The periplasmic, group III catalase of *Vibrio fischeri* is required for normal symbiotic competence and is induced both by oxidative stress and by approach to stationary phase. J Bacteriol 180:2087–2092
Zamocky M, Godocikova J, Gasperik J, Koller F, Polek B (2004) Expression, purification, and sequence analysis of catalase-1 from the soil bacterium *Comamonas terrigena* N3H. Protein Expr Purif 36:115–123
Zamocky M, Koller F (1999) Understanding the structure and function of catalases: clues from molecular evolution and in vitro mutagenesis. Prog Biophys Mol Biol 72:19–66